Advanced Vehicle Hybrid Energy Recovery: A Novel Suspension-Based Electromagnetic and Thermal Harvesting Coupled with Regenerative Braking

Talal Malik[1], *Assad Annis*[1], *Umair Aamir*[2]
[1]NED University of Engineering & Technology (NEDUET), Karachi, Pakistan
[2]San Francisco State University (SFSU)

Abstract

Vehicle suspension systems dissipate substantial mechanical vibrational and thermal energy during normal driving, representing an underutilized opportunity for energy recovery in electric and hybrid vehicles (EVs/HEVs). This study proposes a tri-modal hybrid energy recovery architecture integrating electromagnetic suspension (EMS) harvesting from vertical oscillations, thermoelectric generation (TEG) from damper waste heat, and conventional regenerative braking within a unified power-conditioning framework. Analytical models based on Faraday's law of electromagnetic induction and the Seebeck effect are developed to characterize subsystem performance and are experimentally validated using a scaled quarter-car model. The model incorporates linear electromagnetic harvesting, thermoelectric modules supplied via a controlled thermal gradient, and a DC–DC conversion stage for energy storage in a lead-acid battery. Experimental results indicate that the integrated hybrid configuration yields approximately **120 J** of net usable energy per test cycle, with subsystem contributions of **61% from TEG (73 J), 29% from regenerative braking (35 J), and 10% from EMS harvesting (12 J)**. The reported battery-endurance improvements relative to operation without regeneration were **9.1%** for RBS alone and approximately **27%** for the hybrid configuration. These endurance gains are distinct from the net usable energy ratio: the hybrid total of 120 J is approximately 3.43 times the 35 J attributed to RBS alone. Several subsystem electrical quantities (notably the EMS operating current and the RBS operating voltage/current) are back-calculated from reported power and energy totals rather than independently measured, and the reported 9.1%/27% endurance figures are test outcomes that the accompanying voltage-response plot supports only qualitatively; both caveats are stated explicitly where the corresponding values are derived. Although thermoelectric conversion efficiency ($\sim$5%) and low magnetic field strength ($\sim$0.1 T) impose practical limitations on TED and EMS performance respectively, the results demonstrate that coordinated multi-modal energy harvesting can significantly enhance overall energy recovery potential. The proposed architecture provides a scalable framework for improving energy efficiency and extending effective driving range in next-generation electric vehicles.

Keywords—Energy harvesting; regenerative suspension; thermoelectric generator; electromagnetic damper; regenerative braking; electric vehicles

1 Introduction

The escalating impacts of climate change, coupled with rising global energy needs, are driving a fundamental transformation in the automotive sector toward sustainability. Electric Vehicles and Hybrid Electric Vehicles have emerged as viable alternatives to internal combustion engine vehicles due to their lower carbon footprint and high energy efficiency [1, 2]. However, battery endurance and energy optimization remain core challenges [3]. As the powertrain energy flow management and energy recovery braking systems reach maturity [4, 5], the energy harvesting possibilities from a vehicle suspension are still in early stages [6, 7, 8]. In current EVs, substantial energy is lost during road-induced vibrations, braking, and thermal dissipation through suspension damping. Although regenerative braking has seen broad adoption, energy harvesting from suspension systems and dampers remains largely untapped. Few notable advancements have been made to assess the possibility of harvesting energy from the suspension system. Elliott and Zilletti utilized an electromagnetic transducer as either a shunt damper or an energy harvester [9]. The use of piezoelectric generators has also been discussed as an energy harvester in a vehicle's suspension [10]. Addressing this, a tri-modal regenerative system is designed to harness energy from three major sources of mechanical loss: (1) vertical oscillations via an EMS; (2) heat generated in shock absorbers through Thermoelectric Dampers (TED) using TEGs; and (3) kinetic energy during braking through a Regenerative Braking System (RBS).

This novel design uses thermoelectric generators attached to the damper walls to convert waste heat into useful electrical energy. Thermoelectric generators convert heat to electricity via the thermoelectric effect, offering a silent, eco-friendly solution with typical efficiencies around 5% [11]. The use of TEGs to recover energy from exhaust gases is also under research [12].

One of the core components of this project is the integration of regenerative suspension systems, as they have been theoretically quantified under different conditions [13]. Suspension regenerative systems are categorized, based on their power extraction mechanisms, into two types: (1) DC linear motor, in which viscous dampers with regenerative actuators and rotary electromagnetic dampers are used to harvest energy from vibrations [14]; (2) rotary electromagnetic damper, in which two one-way clutches and a ball-

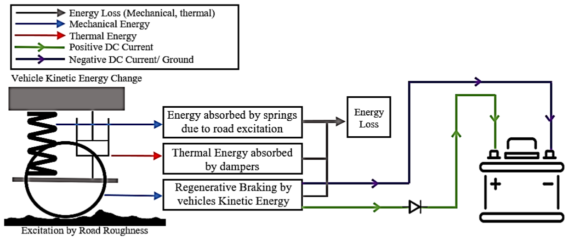

Figure 1: Traditional energy recovery system with only a regenerative braking system.

screw mechanism are used to smoothly convert reciprocating linear motion into unidirectional rotation [15].

Another component of this project is the RBS. This is already widely used in almost all HEVs and EVs. Regenerative braking demonstrates its greatest benefits in urban driving, where approximately 62.5% of energy is dissipated in the Metropolitan driving cycle due to frequent braking. If all braking energy were fully regenerated without losses, fuel consumption could theoretically improve by up to 33% [16]. For instance, a 1000 kg vehicle can achieve theoretical fuel savings of 15% [17]. The goal of this project is to seamlessly integrate the regenerative braking system with the proposed thermo-electromagnetic suspension design. Figure 1 shows the current regenerative system, which is composed only of a regenerative braking system; most of the energy is lost during road excitation and deceleration by means of thermal and mechanical (kinetic and vibrational) forces. This paper proposes an improved design with a hybrid waste-energy regenerative system that recovers a significant portion of energy from the vehicle suspension in addition to the regenerative braking system.

This paper presents a novel approach focused on the conversion of vibrational and thermal dissipation from the suspension system through different kinds of energy-converting modules. Various energy harvesting systems have been investigated, but the integrability of hybrid regenerative systems is rarely discussed. Section 2 studies the suspension system energy conversion mechanism, presents the associated mathematical models, and discusses the integration of the suspension with the RBS and DC–DC converters for efficient power flow, including simulation and experimental verification from a scaled-down prototype. Section 3 presents and discusses the overall experimental results and their feasibility for real-life application. Section 4 concludes the paper.

2 Materials and Methods

2.1 Energy Recovery Mechanism

The energy recovery in this study focused on two primary sources: the suspension system and the braking forces of the vehicle. The braking forces represent the kinetic energy lost during deceleration and braking operations under normal driving conditions, whereas the suspension system offers an opportunity to harvest energy from vertical reciprocations caused by road unevenness. The magnitude of these oscillations depends on the roughness of the road, with the dampers of urban vehicles typically operating within a temperature range of $-40°$C to $130°$C [18]. Vehicle body vibrations generally occur within the frequency range of 1–25 Hz [19], although part of this energy is absorbed by the tires [20]. To capture this otherwise wasted energy, the system integrates an EMS equipped with multiple solenoids and a TED containing Thermoelectric Generators (TEC1-12706), which harvest vibrational and thermal energy, respectively. In addition, an RBS was incorporated to further enhance the overall energy recovery process.

The methodology adopted for this project follows a multi-phase approach. It begins with a detailed review of existing regenerative braking technologies to understand their working principles and limitations, providing a foundation for developing an improved regenerative power model. The project emphasizes the integration of solenoids and thermoelectric generators into both the braking and suspension systems as key components responsible for converting mechanical and thermal energy into electrical power. A model was developed for experimental validation. Owing to budget constraints, the suspension system used a spring constant of 2500 N/m, which is 5% of the full-scale Toyota Corolla suspension stiffness (50,000 N/m). The model represents a quarter-car model, meaning that oscillations from only one suspension and wheel assembly are considered. Furthermore, a 1/20-scale suspension setup with defined stiffness and damping forces was constructed to simulate the operational conditions. Comprehensive data collection and analysis were then performed, with performance evaluation focusing on indicators such as energy recovery efficiency and battery life extension. The power flow diagram of the system is shown in Figure 2.

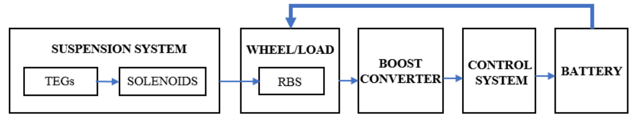

Figure 2: Power flow block diagram.

2.2 Experimental Setup

The model developed in this study was divided into three major subsystems: the mechanical assembly, the booster circuit, and the load and control system. Each subsystem was designed and integrated to replicate the operating conditions of a quarter-car model while ensuring feasibility under laboratory and budget constraints.

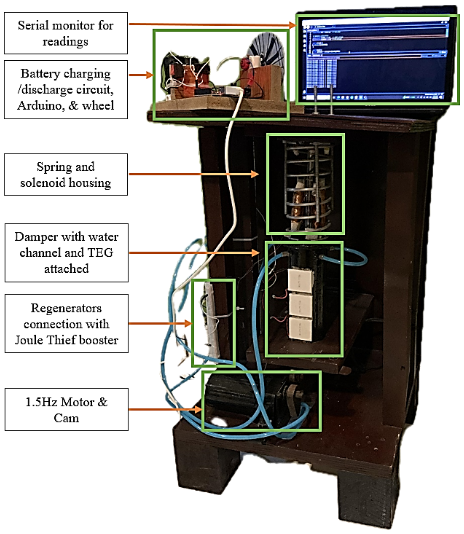

Figure 3: Model of the system.

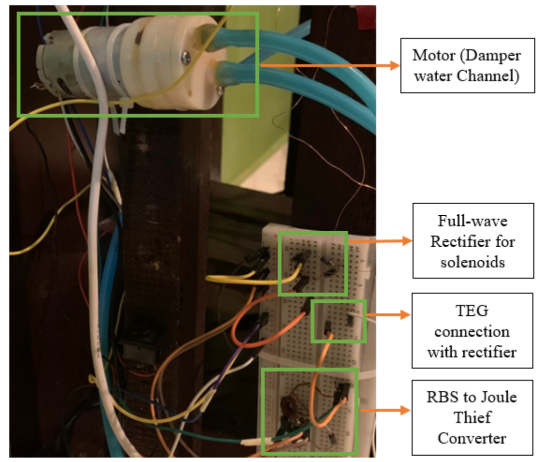

Figure 4: Booster circuit and water pump.

2.2.1 Mechanical

The mechanical assembly is responsible for simulating suspension dynamics and providing the primary energy sources for recovery. A scaled-down spring with a stiffness constant of 2500 N/m, representing approximately 5% of the full-scale Toyota Corolla suspension stiffness (50,000 N/m), was used. The spring stiffness was verified and tested to ensure accuracy and consistency under the experimental conditions. To replicate real-world oscillatory motion, a 1.5 Hz motor was installed at the base of the spring to simulate the reciprocating vibrations experienced by a vehicle suspension system. At the core of the damping unit, a custom-fabricated twin-tube damper adapted from a motorcycle shock absorber was utilized. The inner structure was carefully modified to match the required scale while retaining realistic damping characteristics. Four solenoids were mounted at the base of the damper and connected in series to accumulate a higher voltage output from the vibrational motion. These solenoids act as linear electromagnetic generators, converting reciprocating mechanical energy into electrical energy. To compensate for the insufficient heat generation of the scaled-down damper, four water channels were integrated into the damper. A circulation pump with a flow rate of 1 L/min was employed to regulate the temperature gradient, enabling the TEGs to produce a measurable power output from the thermal domain. This hybrid integration of vibrational and thermal harvesting mechanisms in the mechanical subsystem ensures that both primary sources of suspension-based energy losses are effectively captured. The model is shown in Figure 3.

2.2.2 Booster Circuit

The electrical energy harvested from the solenoids and thermoelectric generators is inherently low in both magnitude and stability, necessitating a voltage-conditioning stage before it can be utilized. To address this, a booster circuit was designed and incorporated into the prototype. The booster circuit comprises a DC–DC step-up converter, optimized to handle fluctuating input voltages ranging from 0.5 to 2 V, typical of the solenoid output, and elevate them to levels suitable for charging storage elements and powering small electronic loads. High-efficiency, low-dropout components were prioritized to ensure minimal conversion losses, as the energy harvested at this scale was limited. A rectification stage precedes the booster module to convert the alternating voltage generated by the solenoids into a unidirectional DC signal. Schottky diodes were used because of their low forward-voltage drop, which reduces power loss during rectification. A similar conditioning approach was applied to the thermoelectric generators, ensuring that both vibrational and thermal sources contributed simultaneously to the energy stream. A smoothing capacitor was placed at the output of the rectifier to stabilize the voltage signal before it entered the booster stage. The overall design of the booster circuit emphasizes reliability, efficiency, and the ability to handle variable input conditions, making it integral to bridging the gap between raw harvested energy and usable electrical power. The system is shown in Figure 4.

2.2.3 Motor Load & Control System

The final stage of the prototype setup involved the load and control system, which managed energy distribution and validated the effectiveness of the harvesting subsystems. The conditioned voltage from the booster circuit was directed to a rechargeable energy storage element consisting of lead-acid battery cells, selected for their stability under repeated charging cycles. A charge-monitoring circuit was integrated to observe the state of charge (SOC) in real time, enabling an accurate evaluation of the contribution of the harvested energy to extending battery life.

In addition to storage, a microcontroller-based control

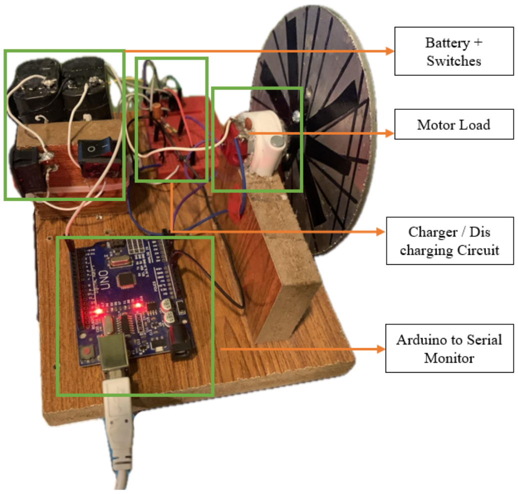

Figure 5: Motor load and control system.

unit was employed to regulate and monitor energy flow, as shown in Figure 5. The Arduino Uno platform was selected for its simplicity and versatility in handling sensor data and control operations. It was tasked with reading the voltages across the storage element, controlling the switching operations, and displaying real-time data for analysis. The load stage also incorporated a low-power resistive and motor-based dummy load to simulate small vehicular subsystems, such as dashboard electronics or auxiliary fans, thereby demonstrating the applicability of the harvested energy for practical automotive functions. Furthermore, the control system allows the logging of critical performance indicators, including voltage stability and battery life improvement. This data-driven approach not only validates the energy recovery capacity of the prototype but also provides a foundation for scaling the system to full-vehicle applications. The integration of storage, monitoring, and regulated load utilization within the control system makes this subsystem a crucial link in demonstrating the viability of hybrid regenerative suspension and braking systems in vehicles.

2.3 Energy Flow in the Hybrid Regenerative System

Figure 6 shows the integration of multiple energy recovery subsystems to enhance the overall efficiency of a vehicle by harvesting energy that is otherwise dissipated as losses. Conventionally, an RBS alone is employed to capture kinetic energy during deceleration; however, this prototype extends recovery potential by incorporating solenoids in the suspension system and TEGs on the damper walls, thereby utilizing both vibrational and thermal domains.

As the vehicle moves over uneven road surfaces, excitations caused by road roughness generate oscillations in the suspension spring. These oscillations are mechanically transferred to the solenoids, inducing AC through electromagnetic induction. Simultaneously, thermal gradients developed in the damper body are absorbed by the TEG modules, converting waste heat into direct current (DC) electricity. The regenerative braking system further contributes by capturing a portion of the vehicle's kinetic energy during braking events.

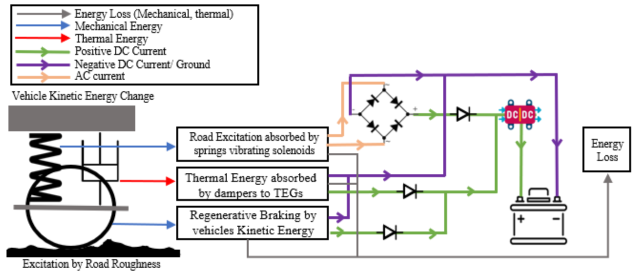

Figure 6: Proposed hybrid regenerative system.

Since the solenoids generate AC, a rectification stage converts this into DC for compatibility with the storage system. To prevent interference between subsystems, blocking diodes are employed, ensuring electrical isolation while allowing parallel contribution from all sources. The rectified outputs are then funneled into a DC–DC booster circuit, which steps up the low, fluctuating voltages from the solenoids and TEGs to higher, stable levels suitable for charging the battery. By conditioning the harvested energy and directing it efficiently to the storage unit, the system minimizes energy loss while maintaining continuous charging capability.

This integrated approach highlights the novelty of combining vibrational, thermal, and kinetic energy recovery in a unified framework, thereby significantly improving the efficiency of regenerative systems beyond conventional braking-only strategies.

2.4 Electromagnetic Suspension System (EMS)

2.4.1 Mathematical Formulation

The EMS operates as a linear electromagnetic energy harvester integrated within the scaled quarter-car suspension assembly. The system consists of four identical solenoids housed within the suspension structure described in Section 2.2.1. Relative motion between a permanent magnet and the solenoid coils, induced by suspension excitation, generates electrical energy based on Faraday's law of electromagnetic induction.

To enable analytical tractability, the following assumptions are adopted:

1. The magnetic field within the effective coil region is spatially uniform.

2. The magnet remains coaxial with the solenoid throughout motion.

3. Core saturation, eddy current losses, and parasitic capacitances are neglected.
4. Electrical loading is purely resistive and matched for maximum power transfer.
5. Mechanical motion of the magnet follows ideal simple harmonic motion.

Governing electromagnetic equations. The instantaneous electromotive force (EMF) induced in a single solenoid is governed by Faraday's law:

$$\varepsilon(t) = -N\frac{d\Phi(t)}{dt} \tag{1}$$

where $\varepsilon(t)$ is the induced EMF (V), N is the number of turns per solenoid, and $\Phi(t)$ is the magnetic flux linking the coil (Wb). The magnetic flux is expressed as

$$\Phi(t) = BA\frac{x(t)}{l_m} \tag{2}$$

where B is the magnetic flux density (T), A is the effective cross-sectional area of the coil (m^2), $x(t)$ is the instantaneous axial displacement of the magnet (m), and l_m is the effective magnet length (m). Differentiating with respect to time yields

$$\frac{d\Phi(t)}{dt} = BA\frac{v(t)}{l_m} \tag{3}$$

Substituting into Faraday's law:

$$\varepsilon(t) = -NBA\frac{v(t)}{l_m} \tag{4}$$

This expression highlights that the induced EMF is directly proportional to magnet velocity rather than displacement.

Mechanical excitation model. The magnet motion is driven by suspension oscillations and is approximated as simple harmonic motion:

$$x(t) = A_0\sin(\omega t), \qquad v(t) = A_0\omega\cos(\omega t) \tag{5}$$

where A_0 is the oscillation amplitude (m), $\omega = 2\pi f$ is the angular frequency (rad$\cdot$s^{-1}), and f is the excitation frequency (Hz). Substituting the velocity expression into the EMF equation gives

$$\varepsilon(t) = -NBA\frac{A_0\omega}{l_m}\cos(\omega t) \tag{6}$$

For a system comprising four solenoids connected in series, the total induced EMF becomes

$$\varepsilon_{total}(t) = 4\,\varepsilon(t) \tag{7}$$

Electrical load model and power generation. Let R_c denote the resistance of a single solenoid. For four solenoids connected in series, the total internal resistance is

$$R_{total} = 4R_c \tag{8}$$

For maximum power transfer, the load resistance is selected as

$$R_{load} = R_{total} \tag{9}$$

The instantaneous circuit current is therefore

$$i(t) = \frac{\varepsilon_{total}(t)}{R_{total} + R_{load}} \tag{10}$$

The voltage across the load is

$$v_{load}(t) = i(t)\,R_{load} \tag{11}$$

The instantaneous electrical power delivered to the load is

$$P(t) = v_{load}(t)\cdot i(t) \tag{12}$$

The average power over one oscillation period T is given by

$$P_{avg} = \frac{1}{T}\int_0^T P(t)\,dt \tag{13}$$

For a sinusoidal EMF waveform, this reduces to

$$P_{avg} = \frac{\varepsilon^2_{total,rms}\,R_{load}}{(R_{total} + R_{load})^2} \tag{14}$$

where $\varepsilon_{total,rms}$ is the root-mean-square value of the total induced EMF of the four series-connected solenoids. This expression gives the power delivered to the external load; the internal coil resistance also dissipates power.

Battery charging model. For a converter receiving average electrical input power P_{in}, power balance gives the average charging current delivered to a battery at approximately constant voltage $V_{battery}$ as

$$I_{charge} \approx \frac{\eta_{conv}\,P_{in}}{V_{battery}} \tag{15}$$

Here η_{conv} denotes conversion efficiency. Setting $\eta_{conv} = 1$ gives the ideal power-balance limit; the reported energy accounting uses an assumed efficiency of 0.80. This relation does not independently determine a measured charging current.

2.4.2 Results and Discussion

Figure 7 illustrates the simulated temporal response of load voltage, load current, and instantaneous power for the four-solenoid EMS operating under ideal matched-load conditions. The simulated waveforms illustrate periodic generation under the assumed excitation and loading conditions; they are distinct from the measured prototype output. However, experimental prototype measurements yielded lower sustained performance due to magnetic field limitations ($\sim$0.1 T), mechanical losses, and non-ideal excitation. For the energy accounting, the reported EMS voltage and average power are retained. The corresponding equivalent current is calculated from power divided by voltage:

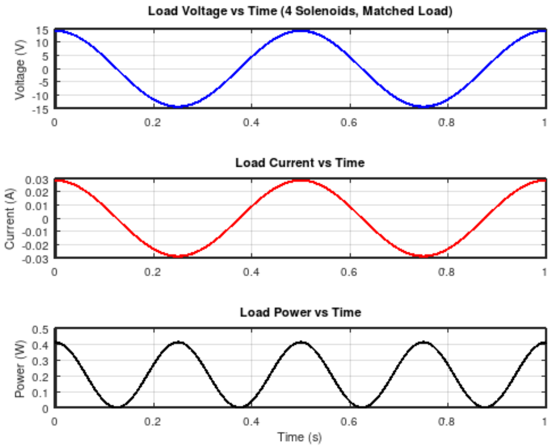

Figure 7: Simulated EMS load voltage, load current, and instantaneous load power for four series-connected solenoids under ideal matched-load conditions.

- Reported DC voltage: 9.0 V
- Calculated equivalent current: $I_{eq} = 0.05/9.0 \approx 0.00556$ A
- Reported average power used for energy accounting: 0.05 W

The equivalent current is an accounting quantity, not a revised current measurement. The previously reported 0.010 A is not used as a corresponding operating current because its product with 9.0 V is 0.090 W, inconsistent with the retained 0.05 W under a steady-DC interpretation. Over a 300 s runtime,

$$\begin{aligned} E_{EMS} &= 0.05 \times 300 = 15 \text{ J}, \\ E_{net} &\approx 12 \text{ J (after 80\% efficiency)} \end{aligned} \tag{16}$$

This confirms that while theoretical EMS performance is higher, practical prototype constraints significantly reduced the harvested power.

2.5 Thermoelectric Dampers (TED)

In the TED, the TEG module (TEC1-12706) was integrated into the suspension damper assembly to harvest thermal energy from the hot–cold differential produced by circulating heated fluid (hot side) and an air-cooled aluminum heat sink (cold side). The working principle is governed by the Seebeck effect, which states that a voltage is generated when two dissimilar semiconductor junctions are subjected to a temperature gradient [11]:

$$V_{oc} = \alpha \Delta T \tag{17}$$

where V_{oc} is the open-circuit voltage (V), α is the Seebeck coefficient of the module (≈ 0.037 V/K for TEC1-12706), and ΔT is the temperature difference between the hot and cold sides of the TEG module (K).

In the present case, the hot side was maintained at ∼73°C and the cold side at ∼64°C, producing a temperature difference of $\Delta T = 9$ K. This yields a theoretical open-circuit voltage per module of

$$V_{oc} = 0.037 \times 9 \approx 0.33 \text{ V} \tag{18}$$

With five modules connected in series, the theoretical open-circuit voltage is approximately

$$V_{oc,total} \approx 1.65 \text{ V} \tag{19}$$

The reported steady-state electrical values for the complete five-module array are listed below; the open-circuit estimate above is a theoretical reference and does not establish the loaded operating point:

- Average voltage (series configuration): 1.65 V
- Average current: 0.185 A
- Average power: 0.305 W

The total harvested (gross) energy over a 300 s runtime was calculated as

$$E = P_{avg} \times t = 0.305 \times 300 \approx 92 \text{ J} \tag{20}$$

Accounting for conversion and booster efficiency ($\eta \approx 0.80$), the net usable energy became

$$E_{net} = 0.305 \times 300 \times 0.80 = 73.2 \text{ J} \approx 73 \text{ J} \tag{21}$$

Thus, the TED subsystem contributes **approximately 61%** of the total net usable energy in the hybrid prototype configuration. The gross value of 92 J is rounded for display; the net value is calculated before rounding.

2.6 Regenerative Braking System (RBS)

The regenerative braking system converts kinetic energy during deceleration into electrical energy. Unlike traditional hydraulic braking, the RBS routes the captured energy back into the electrical storage system, improving the overall energy efficiency of the vehicle.

During braking, the electric motor switches its role to operate as a generator, producing a back EMF proportional to rotational speed. This energy is regulated through a power controller and delivered to the battery or auxiliary systems. The following derivation establishes the electrical quantities for the RBS subsystem consistent with the reported usable energy of 35 J over a 60 s capture window. The calculation is an algebraic consistency check, not an independent measurement of each derived quantity:

$$P_{batt} = \frac{E_{usable}}{t} = \frac{35}{60} = 0.5833 \text{ W} \tag{22}$$

The generator-side (pre-booster) electrical power must compensate for booster losses:

$$P_{elec} = \frac{P_{batt}}{\eta_b} = \frac{0.5833}{0.80} = 0.7292 \text{ W} \approx 0.73 \text{ W} \tag{23}$$

Using the assumed motor (generator) efficiency $\eta_m = 0.75$, the corresponding mechanical input power is estimated as

$$P_{mech} = \frac{P_{elec}}{\eta_m} = \frac{0.7292}{0.75} = 0.9723 \text{ W} \quad (24)$$

The harvested electrical energy over the capture interval is

$$E_{harvest} = P_{elec} \times t = 0.7292 \times 60 = 43.75 \text{ J} \approx 44 \text{ J} \quad (25)$$

Power into the battery relates to battery voltage and battery-side charging current:

$$\begin{aligned} P_{batt} &= V_{batt} \times I_{batt} \\ \Rightarrow\ I_{batt} &= \frac{P_{batt}}{V_{batt}} = \frac{0.5833}{4.10} = 0.1423 \text{ A} \end{aligned} \quad (26)$$

On the generator side, the algebraic constraint is

$$P_{elec} = V_g \times I_g \quad (27)$$

Selecting I_g within the motor operating envelope:

$$I_g = 0.270 \text{ A} \quad (28)$$

Then,

$$V_g = \frac{P_{elec}}{I_g} = \frac{0.7292}{0.270} = 2.70 \text{ V} \quad (29)$$

Verification:

$$P_{elec} = V_g \times I_g = 2.70 \times 0.270 = 0.729 \text{ W} \approx 0.73 \text{ W} \quad (30)$$

$$E_{harvest} = P_{elec} \times t = 0.729 \times 60 = 43.74 \text{ J} \approx 44 \text{ J} \quad (31)$$

$$E_{usable} = E_{harvest} \times \eta_b = 43.74 \times 0.80 = 34.99 \text{ J} \approx 35 \text{ J} \quad (32)$$

System-level contribution relative to the total usable energy ($E_{usable,TED} = 73$ J, $E_{usable,EMS} = 12$ J):

$$\begin{aligned} \text{Contribution}_{RBS} &= \frac{35}{73 + 35 + 12} = \frac{35}{120} \\ &\approx 0.292 \approx 29.2\% \end{aligned} \quad (33)$$

Summary of derived quantities: $V_g = 2.70$ V, $I_g = 0.270$ A, $P_{elec} = 0.73$ W, $E_{harvest} = 44$ J, $E_{usable} = 35$ J, contribution $= 29\%$.

3 Results

3.1 Energy Harvested

Gross electrical energy over the stated operating interval is related to average electrical power by

$$E = P_{avg}\, t \quad (34)$$

where t is the operating time (s). For time-varying signals, average power is the time average of the simultaneous voltage–current product:

$$P_{avg} = \frac{1}{t} \int_0^t v(\tau) i(\tau)\, d\tau = \frac{E}{t} \quad (35)$$

For steady DC operation, this reduces to $P = VI$. In general, the product of separately averaged voltage and current is not necessarily the average power. The retained power values in Table 1 form the basis of the energy calculations. Net usable electrical energy is estimated by applying the assumed conversion efficiency:

$$E_{net} = E \times \eta_{booster} \quad (36)$$

where $\eta_{booster} = 0.80$ (assumed).

The TED supplies the largest share of net usable energy, while the RBS has the highest average power over its shorter capture interval. The EMS adds a smaller contribution. The reported test sequence comprises 300 s of EMS and TED operation and 60 s of RBS capture. The displayed subsystem totals sum to approximately 151 J gross electrical energy and 120 J estimated net usable energy. The net energy shares are 10% EMS, 61% TED, and 29% RBS. Relative to RBS alone, the hybrid net energy is $120/35 \approx 3.43$ times as large; this energy ratio is distinct from the reported battery-endurance improvement.

It should be noted that, owing to the scaled-down nature of the prototype, the damper did not generate sufficient frictional heat to drive the TEG modules independently. To compensate, an external water circulation system was used to maintain the required thermal gradient, as described in Section 2.2.1. Accordingly, the TED results reported here characterize the electrical performance of the thermoelectric subsystem under a controlled, externally imposed thermal gradient, rather than demonstrating that the scaled damper itself generates 73 J of recoverable waste heat under real driving or braking conditions. The TED contribution figures should therefore be read as a subsystem-level characterization and applied cautiously when extrapolating to full-scale, self-generated damper heat in real-world applications.

3.2 Battery Endurance and Voltage Response

Battery endurance was evaluated for operation without regeneration, with RBS alone, and with the hybrid configuration (RBS + EMS + TED). The reported endurance improvements relative to the no-regeneration baseline were 9.1% for RBS alone and approximately 27% for the hybrid configuration. Here, endurance refers to operating duration under the test conditions, rather than battery service life or long-term degradation.

Figure 8 shows battery voltage versus test-cycle number. The RBS curve lies above the no-regeneration curve, and the hybrid curve lies highest, qualitatively supporting the ordering of the reported endurance results. The plot does not independently establish the exact 9.1% and 27% improvements because it does not present the complete endurance durations and common termination criterion needed to reproduce those percentages. The percent-

Table 1: Gross electrical energy, estimated net usable energy, and subsystem contributions over the reported operating intervals.

Subsystem	Avg. DC Voltage (V)	Avg. Current (A)	Avg. Power (W)	Time (s)	Energy (J)	Net Energy (J)	Contribution (%)
EMS	9.00	0.00556[a]	0.05	300	15	12	10%
TED	1.65	0.185	0.305	300	92	73	61%
RBS	2.70	0.270	0.729	60	44	35	29%

[a]EMS current is calculated as P/V and is not an independently measured average current. RBS electrical quantities are the consistent derived values presented in Section 2.6. Net energy uses an assumed conversion efficiency of 0.80; calculations precede rounding. Shares use the displayed net energies, whose sum is 120 J.

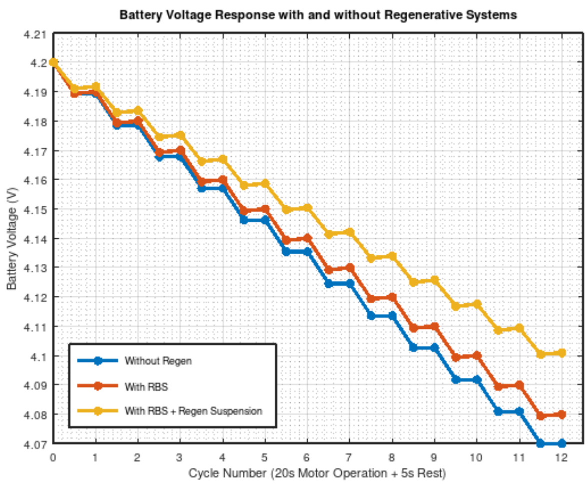

Figure 8: Battery voltage versus test-cycle number without regeneration, with RBS alone, and with the hybrid system (RBS + EMS + TED). Each plotted cycle comprises 20 s of motor operation and 5 s of rest. The curves support a qualitative comparison of voltage retention.

ages are therefore retained as reported test outcomes, not calculated from the plotted voltage differences.

The low thermoelectric conversion efficiency discussed in Section 1 limits absolute electrical output, even though the TED provides the largest relative share of the recovered energy in this prototype. Electromagnetic recovery depends on suspension excitation, while the low magnetic field strength (approximately 0.1 T) and conversion losses further limit net electrical output.

4 Conclusion

This study presented the design, modeling, and prototype evaluation of a hybrid energy recovery system integrating electromagnetic suspension harvesting, thermoelectric generation within the damper assembly, and regenerative braking. The scaled quarter-car prototype retained a spring stiffness of 2500 N/m, corresponding to 5% of the full-scale reference stiffness. Under the reported laboratory conditions, the subsystem energy accounting yielded approximately 151 J gross electrical energy and 120 J estimated net usable energy after applying an assumed conversion efficiency of 0.80. The TED, RBS, and EMS contributions were approximately 73, 35, and 12 J, respectively, corresponding to 61%, 29%, and 10% of the net total.

The reported battery-endurance improvements were 9.1% for RBS alone and approximately 27% for the hybrid configuration, both relative to operation without regeneration. The voltage trajectories qualitatively support this ordering, while the exact percentages remain reported endurance outcomes rather than quantities independently demonstrated by Figure 8. The hybrid-to-RBS net energy ratio of approximately 3.43 is a separate performance metric.

The prototype demonstrates the feasibility of integrating the three recovery pathways under the stated test conditions. Low magnetic field strength, thermoelectric conversion limits, excitation-dependent suspension response, and conversion losses constrain the available electrical output. Future work will focus on magnetic materials, power electronics, and evaluation at larger scales under varied road excitations. Full-vehicle performance requires separate validation; the present results establish prototype-level energy recovery and integration feasibility.

Abbreviations

EMS – Electromagnetic Suspension TED – Thermoelectric Damper TEG – Thermoelectric Generator RBS – Regenerative Braking System UDDS – Urban Dynamometer Driving Schedule SOC – State of Charge EV – Electric Vehicle ICE – Internal Combustion Engine DC – Direct Current AC – Alternating Current α – Seebeck Coefficient ΔT – Temperature Difference V – Voltage I – Current P – Power E – Energy η – Efficiency rpm – Revolutions per Minute kWh – Kilowatt-hour MJ – Megajoule J – Joule W – Watt N – Newton m/s – Meters per Second kg – Kilogram km – Kilometer s – Second avg – Average

References

[1] Muratori, M., Alexander, M., Arent, D., Bazilian, M., Cazzola, P., Dede, E. M., Farrell, J., Gearhart, C., Greene, D., Jenn, A., Keyser, M., Lipman, T., Narumanchi, S., Pesaran, A., Sioshansi, R., Suomalainen, E., Tal, G., Walkowicz, K., & Ward, J. (2021). The rise of electric vehicles—2020 status and future expectations. *Progress in*

Energy, 3(2), 022002. https://doi.org/10.1088/2516-1083/abe0ad

[2] M. Ehsani, K. V. Singh, H. O. Bansal and R. T. Mehrjardi, "State of the Art and Trends in Electric and Hybrid Electric Vehicles," *Proceedings of the IEEE*, vol. 109, no. 6, pp. 967–984, June 2021. https://ieeexplore.ieee.org/document/9422914

[3] G. Suciu and A. Pasat, "Challenges and opportunities for batteries of electric vehicles," *2017 10th International Symposium on Advanced Topics in Electrical Engineering (ATEE)*, Bucharest, Romania, 2017, pp. 113–117. https://ieeexplore.ieee.org/abstract/document/7905058

[4] Chung, C. T., Hung, Y. H. Performance and energy management of a novel full hybrid electric powertrain system. *Energy* 2015;89:626–636. https://ideas.repec.org/a/eee/energy/v89y2015icp626-636.html

[5] Musolino, V., Pievatolo, A., Tironi, E. A statistical approach to electrical storage sizing with application to the recovery of braking energy. *Energy* 2011;36:6697–6704. https://www.researchgate.net/publication/251581918

[6] Xie, X. D., Wang, Q. Energy harvesting from a vehicle suspension system. *Energy* 2015;86:385–392. https://ideas.repec.org/a/eee/energy/v86y2015icp385-392.html

[7] Abdelkareem, M. A. A., Xu, L., Ali, M. K. A., Elagouz, A., Mi, J., Guo, S., Liu, Y., & Zuo, L. (2018). Vibration energy harvesting in automotive suspension system: A detailed review. *Applied Energy*, 229, 672–699. https://doi.org/10.1016/j.apenergy.2018.08.030

[8] Asadi, E., Ribeiro, R., Khamesee, M. B., and Khajepour, A., "A New Adaptive Hybrid Electromagnetic Damper: Modelling, Optimization, and Experiment," *Smart Materials and Structures*, Vol. 24, No. 7, Paper No. 075003, 2015. https://doi.org/10.1088/0964-1726/24/7/075003

[9] Elliott, S. J.; Zilletti, M. Scaling of electromagnetic transducers for shunt damping and energy harvesting. *J. Sound Vib.* 2014, 333, 2185–2195. https://www.researchgate.net/publication/260031565

[10] Xiao, H.; Wang, X.; John, S. A dimensionless analysis of a 2DOF piezoelectric vibration energy harvester. *Mech. Syst. Signal Process.* 2015, 58, 355–375. https://doi.org/10.1016/j.ymssp.2014.12.008

[11] Snyder, G. J. (2009). Thermoelectric Energy Harvesting. In: Priya, S., Inman, D. J. (eds) *Energy Harvesting Technologies*. Springer, Boston, MA. https://doi.org/10.1007/978-0-387-76464-1_11

[12] Krishna Kumar, T. S., Anil Kumar, S., Kodanda Ram, K., Goli, K. R., Prasad, V. S. Analysis of thermo electric generators in automobile applications. *Materials Today: Proceedings* 2021;45(7):5835–5839. https://doi.org/10.1016/j.matpr.2020.08.081

[13] Kim, J. H., Shin, Y. J., Chun, Y. D. et al. Design of 100W Regenerative Vehicle Suspension to Harvest Energy from Road Surfaces. *Int. J. Precis. Eng. Manuf.* 19, 1089–1096 (2018). https://doi.org/10.1007/s12541-018-0129-5

[14] Farbod Khoshnoud, Yuchi Zhang, Ray Shimura, Amir Shahba, Guangming Jin, Georgios Pissanidis, Yong K. Chen, and Clarence W. De Silva, "Energy Regeneration From Suspension Dynamic Modes and Self-Powered Actuation," *IEEE/ASME Transactions on Mechatronics*, Vol. 20 (5): 2513–2524, October 2015. https://doi.org/10.1109/TMECH.2015.2392551

[15] Liu, Y., Xu, L., & Zuo, L. (2017). Design, Modeling, Lab, and Field Tests of a Mechanical-Motion-Rectifier-Based Energy Harvester Using a Ball-Screw Mechanism. *IEEE/ASME Transactions on Mechatronics*, 22(5), 1933–1943. https://doi.org/10.1109/TMECH.2017.2700485

[16] *Energy: Ford Energy Report – Volume 1*. Ford Motor Company, 1981. https://www.fordfoundation.org/wp-content/uploads/2015/05/1981-annual-report.pdf

[17] D. B. Gilmore. *International Journal of Vehicle Design*, 1992, 13(2), 125–133.

[18] Dixon, J. C. *The Shock Absorber Handbook*, Second Edition, John Wiley & Sons, 2007, ISBN: 978-0-470-51020-9.

[19] Lak, M. A., Degrande, G., & Lombaert, G. (2011). The effect of road unevenness on the dynamic vehicle response and ground-borne vibrations due to road traffic. *Soil Dynamics and Earthquake Engineering*, 31(10), 1357–1377. https://doi.org/10.1016/j.soildyn.2011.04.009

[20] Durand-Gasselin, B., Dailliez, T., Mössner-Beigel, M., Knorr, S., Rauh, J. Assessing the thermo-mechanical TaMeTirE model in offline vehicle simulation and driving simulator tests. *Veh.*

Syst. Dyn. 2010;48(Suppl):211–229. https://doi.org/10.1080/00423111003706730